

1 the cathode, providing a facile pathway for ion movement. Unlike one-dimensional (1D)
2 binders, the unique 3D hierarchical structure exhibits multi-dimensional bonding
3 interactions with active materials and therefore offers robust contacts between both
4 components. When the active material loses its original contact with the binder during
5 potential cycling, CPB can successfully recover its 3D hierarchical network, thus
6 creating a self-healing effect. CPB-based LiFePO₄ electrode shows remarkably
7 improved electrochemical performances compared to other well-known binders, such
8 as poly(vinylidene fluoride).

9 **Keywords:** 3D hierarchical nanostructures; Walnut kernel shape; Conductive polymer;
10 Water soluble binder; Lithium-ion battery.

11 **1. Introduction**

12 Driven by the strong and ever-growing demand for miniaturization of portable
13 energy storage devices (ESD), it is now becoming necessary to develop small and
14 reliable energy storage with high energy density, long-term durability and high safety.

15 Although lithium-ion batteries (LIBs) have been the predominant commercial ESDs for
16 some time, they cannot sufficiently satisfy long-term storage requirement because of
17 their inherent limitation of energy density [1, 2]. Researchers have made substantial
18 efforts in researching and developing active materials, separators and electrolytes to
19 enhance the energy density [3]. However, little attention has been paid to develop novel
20 LIB auxiliary materials, such as the binder. In fact, the binder plays an important role
21 in a LIB as it binds the active materials onto the current collector [4, 5]. An ideal binder

1 should be of low cost, strong bonding, high physical and electrochemical stability in
2 the electrolyte [6].

3 The binders used in LIBs are generally made of high molecular polymers, which can
4 be divided into two categories: organic solvent-based binders and aqueous binders [7].
5 Poly(vinylidene fluoride) (PVDF), an organic solvent-based binder material, has been
6 commercially and extensively used as a LIB cathode binder even though this polymer
7 possesses unfavorable characteristics in LiFePO_4 due to its non-conductive defect and
8 large volume change during Li^+ insertion/extraction process, as well as its negative
9 effect on the environment and high cost [8-10]. To address these issues, the
10 development of water-soluble binders has become a new growing area of LIB
11 technology. Early works on binders mainly focus on gelatin [4], polyvinyl alcohol (PVA)
12 [11], carboxyl methylated cellulose (CMC) [12, 13], CMC/styrenebutadiene rubber
13 (SBR) [12, 14], poly(ethylene oxide) (PEO) [15], chitosan [9] and others [8, 16-20].
14 CMC materials have attracted a lot of attention as they open up a new area for water-
15 based processes for LIB electrode manufacturing. Although CMC is usually used
16 together with SBR to obtain better cell performances, it can only be used for the
17 preparation of negative electrodes under a reducing atmosphere due to its
18 electrochemical instability [14].

19 In the development of higher energy and power density LIB, the choice of the binder
20 (and its physicochemical properties) is important and therefore should not affect the
21 performance and durability of the overall battery. Conventional non-conductive water-
22 soluble binders display insulating characteristics as they possess **non-conductive**

1 functional groups of polymers and the chemical structure yielding poor electrical
2 connections. During the charge-discharge cycling process (Fig. 1a), the active materials
3 suffer from large volume expansion, in turns pushing away the conducting additive
4 from them. Therefore, besides the strong binding capability, an excellent water-based
5 binder should possess the electronic and ionic conductivity at the active material
6 particles surface/electrolyte interface [21]. Elegant studies have shown that the
7 electrochemical performances of LIBs are greatly improved through careful binder
8 design [5, 18, 22-27]. Excellent studies on lithiated ionomers as binders have shown
9 that they can potentially offer a route to enhance ionic conductivity and Li^+ diffusion.
10 Li *et al.* used polyacrylic acid (PAA) as a binder to lower the interphase and charge
11 transfer resistance of LiFePO_4 cathodes [28]. Xue *et al.* prepared a LiFePO_4 cathode
12 with the Li^+ form of a perfluorosulfonate ionomer as a binder to compensate for the
13 electrolyte depletion from the electrode porous space during rapid discharging. Due to
14 the weak adhesive strength of pure lithiated poly(perfluoroalkyl-sulfonyl)imide
15 (PFSILi), PVDF was introduced to hinder the crystallinity and enhance the adhesion of
16 the composite binder [27]. The rate of Li^+ transport inside the active materials and in
17 the porous space of the electrode, as well as the interface between the electrode and the
18 electrolyte, plays an essential role during the charge-discharge cycling process, and
19 even in part, determining the overall battery performance. However, it has been pointed
20 out that most conducting ionomer has unsatisfactory adhesion properties, thus the
21 balance between bonding strength and conductivity needs to be further explored.

22 Owing to the delocalization of the negative charge in the polymer, the anion has been

1 incorporated in a polyanionic block co-polymer as the functional pendant group to
2 prepare binders for LIBs. Developing an ‘effective conductive network structure’ with
3 excellent adhesion is the key objective for desirable binding materials. Very recently, a
4 water-based latex assembly technique has been shown to be an effective way to
5 fabricate conducting nanocomposites with 3D and interconnected networks [29, 30].
6 Specifically, polymer latex was mixed uniformly with a conducting carrier yielding a
7 well-dispersed binder mix. During this process, conducting carrier was selectively
8 located in the interstitial space between the polymer latex microspheres and assembled
9 into a continuous 3D hierarchical network.

10 In this study, a unique 3D hierarchical water-based polymer binder was produced
11 from the esteryl-enriched/cyano-enriched monomers and introducing a sulfo-anion into
12 them. The walnut kernel shape 3D hierarchical structure was induced by the latex self-
13 assembly through the interaction between the hydrophilic segment and the hydrophobic
14 blocks in conjunction with the electrostatic repulsion of the sulfonate groups and steric
15 hindrance of large side groups; in turns ensuring constant adhesion and electrical
16 connections even when the electrode integrity was damaged during the charge-
17 discharge cycling process (Fig.1b). This unique structure endowed the CPB with
18 excellent adhesion and rapid transport of Li^+ . Based on the known structural features of
19 the material, the feasibility of using the CPB as the positive electrode for LIBs was
20 investigated with a focus on ionic conductivity, electrochemical stability, cell
21 performances with LiFePO_4 as cathode and Li as anode.

22 **2. Experimental section**

1 *2.1 Synthesis of CPB*

2 Acrylic acid *n*-butyl ester (BA), acrylonitrile (AN) and ammonium persulfate (APS)
3 were obtained from Sinopharm Chemical Reagent Co., Ltd, China. 2-Acrylamido-2-
4 methylpropanesulfonic acid (AMPS) was obtained from J&K Scientific Ltd and
5 neutralized with LiOH·H₂O before use. All reagents were of analytical grade (AR) and
6 all monomers were thoroughly distilled to remove any traces of polymerization
7 inhibitor prior to use. The conducting polymer binder was prepared by the emulsion co-
8 polymerization method. The monomers were mixed using the following ratio of AMPS:
9 BA: AN = 1:4:4 (in mass) with addition of the initiator. The mixture made of monomers
10 was added into a four-neck bottle under stirring conditions and nitrogen atmosphere
11 and the reaction was kept under reflux at 70°C for 8h. Then, the temperature was
12 increased to 85°C for 2h under reflux to remove any residual monomers and initiator.
13 The addition of the APS was 0.5 wt% of the total monomer. The final obtained
14 conducting polymer binder was labeled as CPB.

15 *2.2 Electrode and cell preparation*

16 The working electrode (WE) slurry was composed of LiFePO₄ (90wt.%), the
17 conducting carbon (5wt.%, Super P, TIMCAL), and the prepared binder (5 wt.%) in
18 water. The WE was prepared by casting the electrode slurry on an Al foil before drying
19 at 100°C for 12h in vacuum. For comparison purposes, a commercial PVDF was used
20 and mixed (as 5wt.%) with the conducting carbon Super P (5wt.%). The loading of the
21 CPB-based and PVDF-based electrodes was about 4.2 mg/cm². A unit cell (2032-type
22 coin) was assembled by sandwiching a Celgard 2400 separator between a lithium anode

1 and a LiFePO_4 cathode using the liquid electrolyte solution, 1M LiPF_6 in ethylene
2 carbonate (EC)/dimethyl carbonate (DMC)/diethyl carbonate (DEC) (1:1:1, v/v/v) in
3 an Argon-filled glove box (Mikrouna Super1220, China).

4 *2.3 Physical characterization*

5 The surface morphologies of the samples were investigated by scanning electron
6 microscopy (SEM) using a FEI Nova Nano SEM 450 operated at 0.5kV in the absence
7 of gold under CBS mode. In all electrode samples, the solid content slurry of PVDF-
8 based and CPB-based was ca. 30%. The chemical bond and functional groups of the
9 polymer were characterized by Fourier transform infrared (FT-IR, Spectrum One,
10 Perkin-Elmer). Adhesion (bond strength or adhesive strength) of the electrode layers
11 onto the Al current collectors were evaluated using a universal tensile tester (Intelligent
12 electronic tensile testing machine, XLW(PC)) operating at a scan rate of 30 cm min^{-1} .
13 The mechanical stretchability of the CPB membrane was measured via a universal
14 tensile tester (XLW(PC)), where samples were subjected to repeated bending stress at
15 a strain rate of 25 mm min^{-1} . For the mechanical strength tests, all samples were ca.
16 2cm in width, 5cm in length and $100 \mu\text{m}$ in thickness. The CPB membrane was
17 fabricated by casting the emulsion onto a clear polyethylene terephthalate (PET)
18 substrate using an automatic coating machine (AFA-III, Hefei Kejing Materials
19 Technology Co., LTD with temperature control). The PVDF membrane was also
20 obtained by casting the PVDF and NMP solution (5wt.%) onto a clear PET substrate
21 using an automatic coating machine (AFA-III). The CPB and PVDF membranes were
22 obtained by peeling off the substrate and drying in a vacuum oven for 24h at 70 and

1 100 °C, respectively. The swelling properties of the binders were examined from mass
2 gain of the electrodes after soaking in the electrolyte for 72h. Thermogravimetric
3 analysis (TGA) was tested on a NETZSCHTG 209 F1 under nitrogen atmosphere at a
4 flow rate of 50mL/min⁻¹ with a heating rate of 10°C min⁻¹ from 40 to 600°C. Differential
5 scanning calorimetry (DSC) was performed using a TA Instruments-Waters LLC under
6 N₂ atmosphere at a flow rate of 50 mL min⁻¹, in the temperature range of -70 to +110
7 °C with a heating rate of 10°C min⁻¹. XRD spectra were recorded by using a Tongda
8 DX-2700 X-Ray power diffractometer (China) with a CuK α radiation.

9 *2.4 Electrochemical measurements*

10 The electrochemical stability of the CPB membrane (saturated with liquid electrolyte)
11 and PVDF membrane (saturated with liquid electrolyte) was evaluated by cyclic
12 voltammetry (CV) using an Autolab Potentiostat/Galvanostat PGStat302N (Metrohm).
13 A three-electrode compartment cell was used. A working and reference electrode was
14 used as stainless steel (SS) and lithium-metal, respectively. All CVs were performed at
15 a scan rate of 0.02 mV s⁻¹. All potentials are referred *vs.* Li/Li⁺. The ionic conductivity
16 of the CPB membrane (saturated with liquid electrolyte) was determined using the
17 symmetrical cell SS/CPB/SS by electrochemical impedance spectroscopy (EIS) (the
18 Autolab Potentiostat/Galvanostat PGStat302N) over the frequency range of 0.1–10⁶Hz
19 with an amplitude of +10 mV, at open circuit voltage (OCV) and at 25°C. For
20 comparison purposes, the ionic conductivity of the PVDF membrane (saturated with
21 liquid electrolyte) was determined under similar conditions. The ionic conductivity was
22 calculated using Equation (1):

1
$$\sigma = \frac{d}{A \cdot R_{0,el}} (1)$$

2 where d and A are thickness and area of the polymer electrolyte, respectively, and $R_{0,el}$
3 is the bulk electrolyte resistance obtained from the EIS spectra. The $R_{0,el}$ and d are
4 obtained by Zview-Zplot software and thickness tester (Labthink, CHY-C2A),
5 respectively. The electrochemical performances were examined using a battery cycling
6 tester (Land CT2001A Battery Tester, China). The cells were cycled at a constant
7 voltage constant current charge/discharge current density between +2.8 and +4.2 V (vs.
8 Li/Li⁺) for the LiFePO₄ cathode. All electrochemical measurements were performed at
9 25 °C.

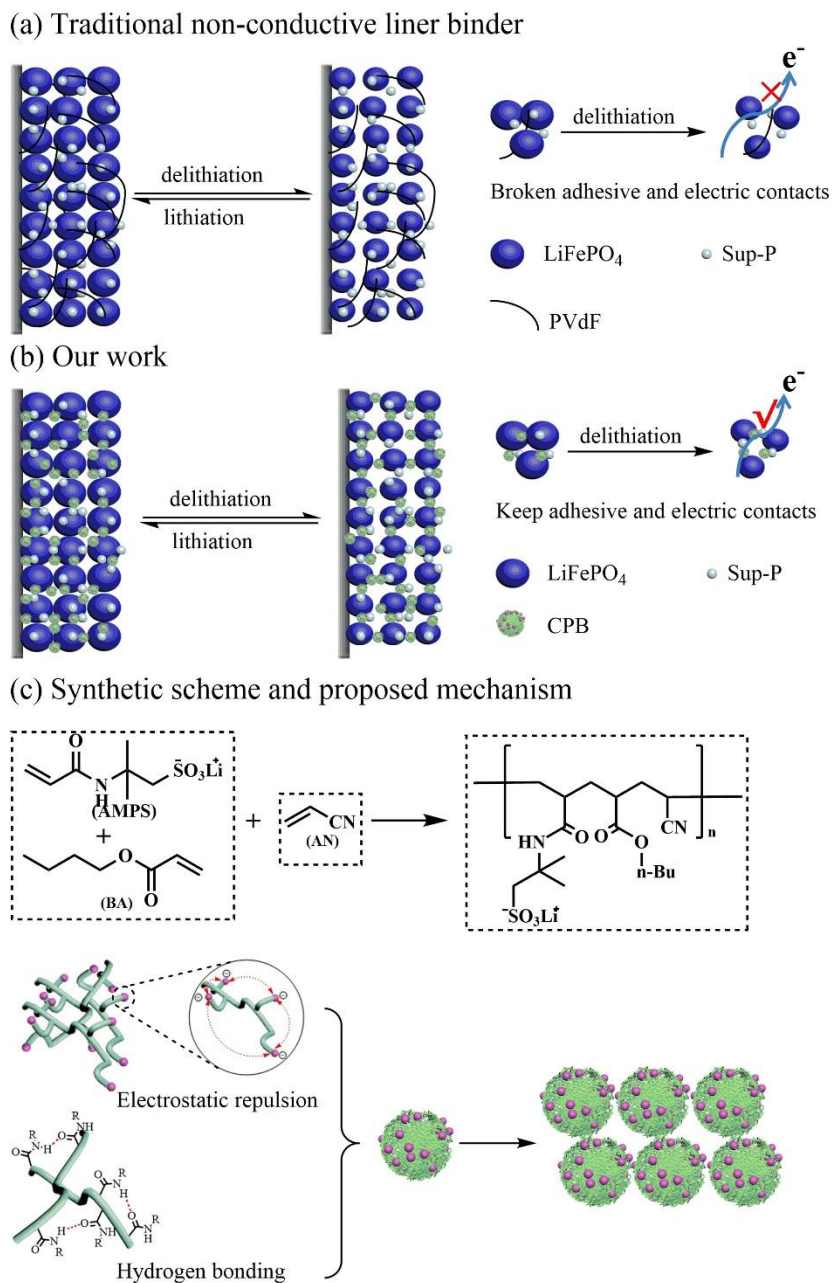
10 **3. Results and discussion**

11 *3.1 Characteristics of the CPB as a flexible conductive binder*

12 *3.1.1 Preparation and FTIR*

13 The schematic illustration of the 3D hierarchical walnut kernel shape conducting
14 polymer binder fabricated by emulsion polymerization of AMPS, BA and AN is
15 presented in Fig.1c. AMPS and BA monomer molecules were added into the solvent-
16 water solution under stirring condition and nitrogen atmosphere in a four-neck bottle;
17 and the reaction was kept under reflux at 70°C for 8h. During the heating process,
18 primary radicals were initiated by thermal decomposition of APS (used as initiator) and
19 the co-polymer was formed by the opening of the double bonds in the vinyl monomers.
20 After 4h of polymerization, a colourless, transparent and flowing characteristic co-
21 polymer P(AMPS-BA) was produced (Fig. S1). Subsequently, AN was added to the as-

1 prepared co-polymer to sustain the polymerization reaction. As the reaction went on,
2 the molecular weight of the P(AMPS-BA-AN) increased. Generally, the neutral
3 polymer that has the attractive interaction sites tends to be entangled by itself due to
4 strong intramolecular interactions. For this reason, aggregation of P(AMPS-BA-AN)
5 will inevitably form through the intramolecular hydrogen bonding (Fig 1c), which
6 deteriorates its interaction with other neighboring polymer chains. In contrast, the
7 polymer P(AMPS-BA-AN) could be stretched because its carboxylates ($-\text{SO}_3^-$) impart
8 the Coulombic repulsion (Fig 1c) [31]. According to the *DLVO* theory, two forces were
9 taken into consideration: the van der Waals attractive force and the electric repulsive
10 force between two adjacent particles due to the overlap of the electric double layer
11 (EDL) of counterions. The van der Waals force makes particles attract with each other,
12 but the electric repulsive force of EDL do the reverse. As the repulsive force is stronger
13 than the attractive force, the particles will disperse in the medium and form a suspension,
14 otherwise aggregation will inevitably appear [32]. Therefore, the combination of these
15 two interaction forces could exhibit a mutually beneficial outcome in a way that the
16 coulombic repulsion diminishes the agglomeration, as well as the phase segregation of
17 the polymer P(AMPS-BA-AN) and the solvent resulting in a more uniformly
18 distributed and continuous 3D hierarchical polymeric network.



1

2 **Fig.1.** Schematics of the approaches to address electrode integrity issue in battery

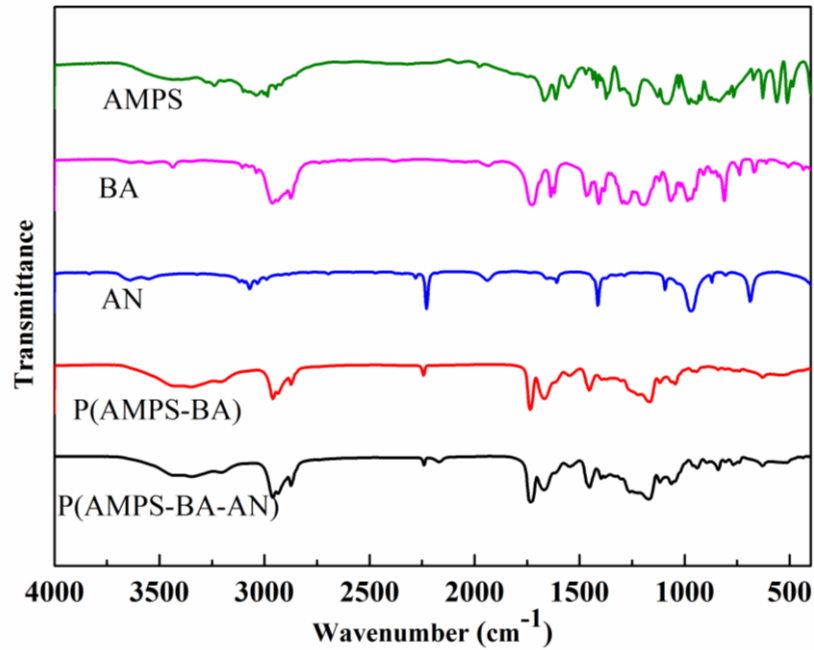
3 materials. (a) Traditional approaches using PVDF as non-conductive polymer binder.

4 (b) Replacing one-dimensional binder or two-dimensional binder, 3D conductive

5 binder could keep the electrical and mechanical integrity of the electrode during

6 charge/discharge cycles. (c) Schematic illustration of the synthesis and proposed

7 mechanism of the conductive polymer binder (CPB) in this study.



1

2 **Fig.2.** FT-IR spectra of P(AMPS-BA-AN) copolymer, P(AMPS-BA), and its
 3 monomers of AN, BA and AMPS.

4 Fig. 2 shows the FT-IR spectra of the binder, intermediate products and monomers,
 5 namely: P(AMPS-BA-AN), P(AMPS-BA), AMPS, BA and AN. The C=C stretching
 6 vibration peaks at 2,920, 1,640, 990 and 920 cm⁻¹ were observed for all monomers. A
 7 CH₂ asymmetric stretching at 2,939 cm⁻¹ was observed for AMPS. The vibrational
 8 bands between 980 cm⁻¹, 1,050 cm⁻¹ and 1,200 cm⁻¹ can be attributed to the sulfonate
 9 group (—SO₃⁻) in AMPS [33]. For the BA monomer, the peaks at 1,630 cm⁻¹ and 1,760
 10 cm⁻¹ may be ascribed to the functional groups of C=C and C=O [34]. The absorption
 11 peaks at 1,619 and 2,239 cm⁻¹ in the AN monomer correspond to the C=C and C≡N
 12 bonds, respectively [35]. Comparing the FT-IR spectrum of the copolymer P(AMPS-
 13 BA) with the monomers, it can be observed that the co-polymer still shows (and remains)
 14 its absorption peaks at 1,760 cm⁻¹ (bond C=O), 980 cm⁻¹, 1,050 cm⁻¹ and 1,200 cm⁻¹

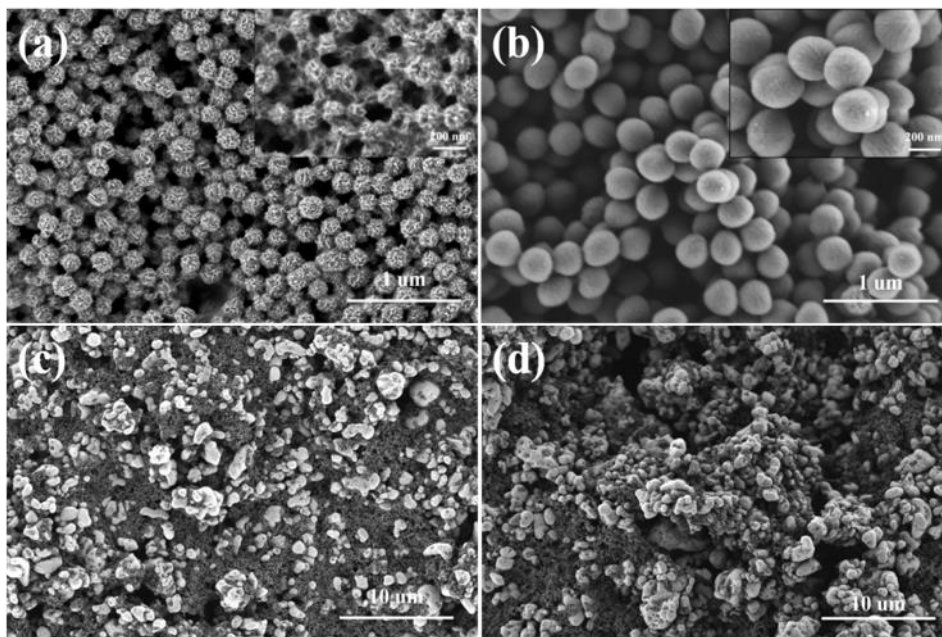
1 ($-\text{SO}_3^-$), but loses the absorption peaks at 1,640, 990 and 920 cm^{-1} for each monomer
2 $\text{C}=\text{C}$ groups. In the case of the P(AMPS-BA-AN), the main absorbance band at 1,720
3 cm^{-1} can be assigned to the $\text{C}=\text{O}$ bond with a characteristic peak at 2,241 cm^{-1}
4 corresponding to the $-\text{C}\equiv\text{N}$ group. The absorption bands at 2,942 and 1,450 cm^{-1} may
5 be attributed to the stretching vibration bands of $-\text{CH}_2$ groups and $-\text{CH}$ bending,
6 respectively [5]. These results indicate that the P(AMPS-BA-AN) is obtained by the
7 way of the breaking each monomer's double bonds $\text{C}=\text{C}$, while maintains the main
8 characteristics of the monomers. The wide and strong vibrational bands at 1,180 and
9 880 cm^{-1} are ascribed to the stretching frequencies of CF_2 in the PVDF (Fig.S2), and
10 the bands at 973, 879, 840, 762, 612 cm^{-1} correspond to the crystallization peaks. These
11 observations are in good agreement with those highlighted by Peng *et al.* [36]. The
12 differences in the molecular structures may highly influence the binding abilities of the
13 binders.

14 3.1.2 Adhesion properties, DSC and mechanical stretchability

15 A binder possessing high adhesion properties plays an important role in improving
16 the electrode performance especially the cycling ability. The adhesive strength values
17 to the aluminum current collectors for the LiFePO_4 electrodes based on PVDF and CPB
18 were 0.33 N cm^{-1} and 1.4 N cm^{-1} , respectively. The load to peel the PVDF -based
19 electrode from the current collector was in accordance with Li's work [17]. It was found
20 that the adhesive strength of CPB system was 4 times higher than that of PVDF. The
21 prepared CPB exhibited a series of nitrile and ether groups, which were physically
22 entangled to each other, leading to the generation of areas of multi-dimensional contacts

1 with the active materials and the conducting agents via non-covalent interactions (such
2 as nitrile bonding and van der Waals forces) [28, 32]. The formation of the 3D
3 hierarchical walnut kernel shape helped in keeping intimate contacts between the active
4 material particles and the multi-dimensional binder during the discharge/charge cycling
5 process. These multi-dimensional interactions exhibited robust adhesion with the active
6 material particles, conducting particles and the current collector. Once the active
7 material or/and conducting particles **loses** their original contacts with the binder during
8 the charge/discharge cycling process, it was found that they could recover the
9 interaction within the multi-dimensional binder in other areas, thus creating a self-
10 healing process and improving the stability of the electrode [31, 37]. It was also found
11 that reducing the amount of the binder in the electrode could enhance the specific
12 energy of the LIBs [38]. Moreover, the $-\text{SO}_3^-$ introduced in the CPB could deliver Li^+
13 during the charge/discharge cycling process due to the electrostatic interaction,
14 resulting in good cycling performance [39]. For PVDF, the bonding ability originates
15 from the formation of **weak bonds** with F atoms and the active materials. **PVDF is easily**
16 **swollen by electrolyte, leading to the penetration of electrolyte solution into the**
17 **electrode and desquamation of electrode particles, therefore, the electrical conductive**
18 **network in the electrode might be in part loosen or broken by the inordinate penetration**
19 **of the electrolyte during cycling [40].** In our conditions, the designed and *as*-prepared
20 binder possesses an amorphous structure with a low glass transition temperature (T_g)
21 (Fig.S3a). The DSC shows that the CPB has two T_g , with one of them around 0 °C, i.e.
22 at a temperature much lower than room temperature. The mechanical stretchability of

1 CPB and PVDF was also investigated. As shown in Fig. S3b, the CPB can be stretched
2 up to ten times its initial length without breaking. In comparison, PVDF shows a much
3 lower stretchability (up to 10%). If there is a crack or a mechanical damage, the
4 amorphous structure, the low T_g and the excellent mechanical stretchability of the CPB
5 allow the polymer chains at the fractured interfaces to rearrange and to intermix. This
6 process is mainly driven by the dynamic reassociation of the hydrogen bonds at room
7 temperature leading to spontaneous self-healing [31, 41]. **During the experiment, it is**
8 **found that the self-healing does not have observable effect on the elasticity and**
9 **mechanical stability of CPB film.**



10

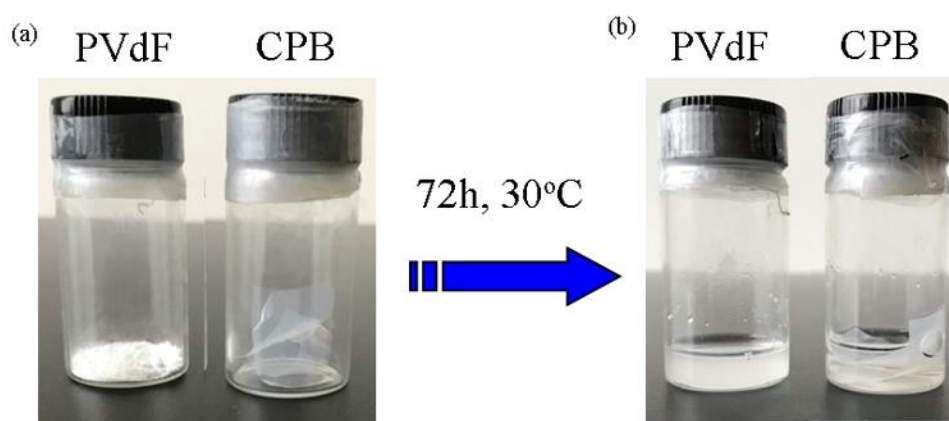
11 **Fig.3.** SEM images for the surface of SEM images of CPB (a) and PVDF (b) and
12 LiFePO_4 electrodes with CPB (c) and PVDF (d) before cycling.

12

13 3.1.3 SEM images

14 It can be observed from Fig.3a that the CPB possesses a 3D hierarchical walnut
15 kernel shape structure **with quite rough surface**, whereas the PVDF is made of small

1 spherical particles (Fig.3b). PVDF is the most widely used commercialized binder for
2 LiFePO_4 in commercial LIBs because of its good adhesion to the electrode materials
3 and current collector, as well as the good dispersion of active materials and conductive
4 agents. Fig. 3c and d shows the SEM images of LiFePO_4 electrodes using two different
5 binder materials after drying at 100°C for 12h in vacuum, respectively. It can be seen
6 that both the cathodes made with PVDF and CPB binder show similar dispersion of
7 LiFePO_4 particles. No big aggregate particles can be found. The crystallinities of the
8 two binders were examined by XRD (Fig.S4). The diffraction peak for PVDF is sharper
9 than that of CPB, revealing that the PVDF has a better crystallinity than CPB [17]. The
10 SEM image suggests that PVDF has regular shape, which is also one of the feature of
11 crystal. The main chains of the PVDF are in part bundled together to form the crystallite
12 region during drying. In the case of CPB, the amorphous polymer characteristics in
13 conjunction with the lower T_g can present viscous flow state when heated, which is help
14 to disperse the active materials and conducting agent.



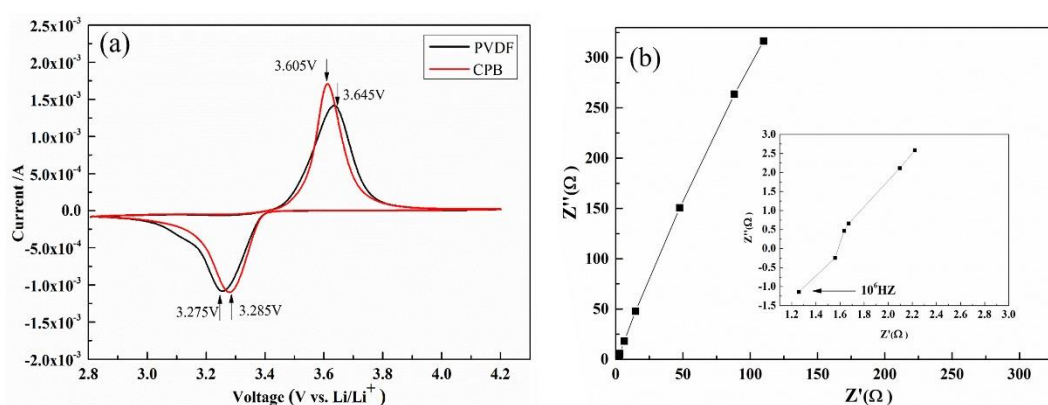
15
16 **Fig. 4.** Visual examination of the interaction between the PVDF and CPB and the
17 electrolyte solution (1mol L^{-1} LiPF_6 dissolved in EC/DMC/EMC 1:1:1 by mass)

1 before and after 72h at 30°C.

2 3.1.4 Swelling property and TGA

3 Swelling property of the binder films were examined by soaking in an electrolyte
4 solution at 30°C for 72h. The binder films were of 14 mm in diameter. The films were
5 weighed (m_1) after removing the electrolyte on the surface with the filter papers. Here,
6 we define the initial mass of the electrode as m_0 . The increased mass percent of the
7 binder films is given by $[(m_1 - m_0)/m_0 \times 100\%]$. In our experimental conditions, the
8 mass gain of the polymer films by the absorption of the electrolyte solution were 20.8%
9 and 15.2% of the initial mass for the PVDF and CPB systems, respectively. The
10 interactions between the CPB and the PVDF (used for comparison purposes) binders in
11 the electrolyte, were inspected visually before and after 72h at 30°C in an Ar-filled
12 glove box (Fig.4). It was observed that after 72h, the PVDF was swollen, forming a
13 viscous, gel-like product, an observation which is in accordance with previous reports
14 [17]. PVDF, a liner polymer, binds the active materials and conducting agents through
15 the weak bond of C-F [42, 43]. The particles in the PVDF-based electrode is lack of
16 long-range connections, resulting in the desquamation of the electrode particles during
17 the charge-discharge process and consequent capacity-fading and cycle life shortening
18 [40, 42, 44, 45]. In contrast, it was found that CPB did not swell under similar
19 experimental conditions, i.e. the CPB was still self-standing and mechanical stable.
20 Therefore, for CPB binder electrode, the polymer can effectively prevent the excessive
21 penetration of the electrolyte and improve the cycling performance compare to the
22 PVDF system.

1 The thermal stability of the PVDF and CPB was determined by TGA. As shown in
 2 Fig.S5, the initial mass loss starts at $\sim 230^{\circ}\text{C}$ with a peak at 260°C for CPB, where the
 3 evolution of a complex peak is clearly observed. The following peak starts from $\sim 320^{\circ}\text{C}$
 4 with a peak at around 365°C , which is in good agreement with the thermal degradation
 5 of the co-polymer P(AMPS-BA-AN). For PVDF, the initial mass loss starts at $\sim 380^{\circ}\text{C}$
 6 with a peak at 455°C . The TGA analysis demonstrates that CPB can withstand
 7 temperatures of up to 180°C without undergoing thermal decomposition and meet the
 8 requirements of practical application for LIBs [46-48].



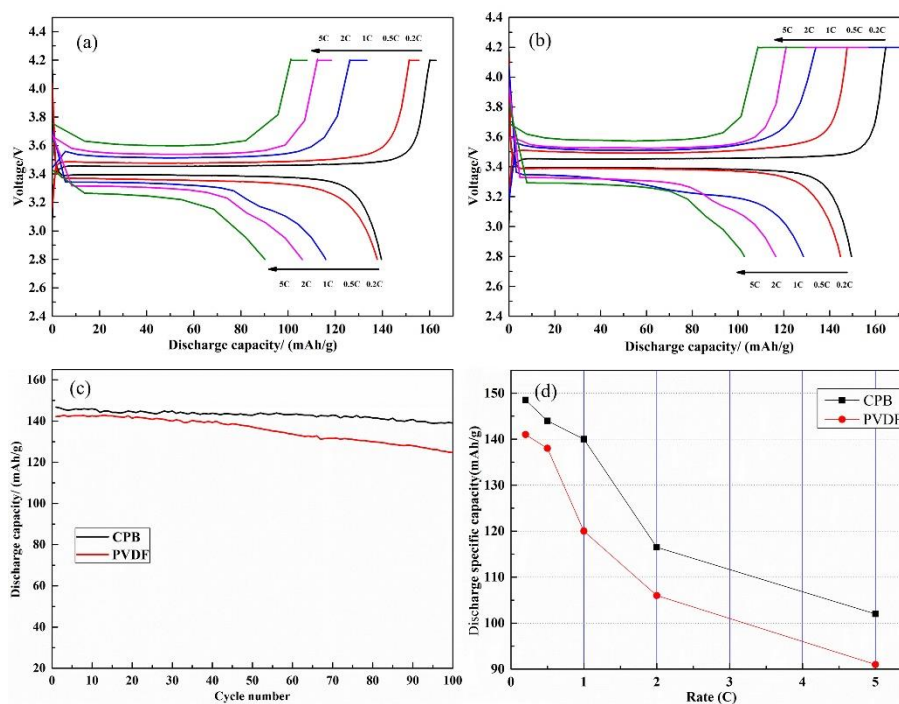
9
 10 **Fig. 5.** Cyclic voltammogram of the LiFePO_4 electrode with CPB and PVDF binders
 11 between $+2.8$ and $+4.2$ V (vs. Li/Li^+) at a scan rate of 0.02 mVs^{-1} and at room
 12 temperature (a); Nyquist plot (EIS) for the CPB membrane with the cell structure of
 13 SS/membrane/SS at room temperature (b).

14 3.2 Electrochemical performances

15 3.2.1 Cyclic voltammograms and ionic conductivity

16 Cyclic voltammograms of the LiFePO_4 electrodes for both PVDF and CPB are
 17 shown in Fig. 5a. The shapes of the two CVs are similar, indicating that CPB does not

1 participate in the electrochemical reaction in the potential window of [+2.8 to +4.2V
2 (vs. Li/Li⁺)]. It can be observed from the figure that the reversible redox couple peaks
3 in the range of +3.290 and +3.605 V (vs. Li/Li⁺) are obtained, corresponding to the
4 embedding and emergence process of the lithium ion in the anode electrode. The
5 electrode prepared with the CPB exhibits a smaller difference between the oxidation
6 and reduction peak potentials (ΔE_p), i.e., +0.32V (vs. Li/Li⁺), than that of PVDF, in
7 which the peak potential difference is +0.37V (vs. Li/Li⁺), which is in good agreement
8 with Cai's work [28]. Moreover, it can be seen that the current is slightly increased and
9 the reduction peak of the LiFePO₄ with PVDF is wide with a low peak current of 1.3mA.
10 In the case of LiFePO₄ with CPB, the peak current is narrow with a slightly higher peak
11 current (1.7mA). These observations may suggest that by changing the binders, the
12 charge-transfer kinetics is enhanced, indicating that the electrode prepared in aqueous
13 solvent by using a CPB exhibits better reversibility and lower polarization, which can
14 be ascribed to the lower resistance of solid electrolyte interphase (SEI) on LiFePO₄ and
15 charge transfer for lithium ion intercalation and de-intercalation.



1

2 **Fig.6.** Electrochemical performances of LiFePO₄/PP/Li with different binders. (a)

3 Charge- discharge curves of PVDF-based cathode at various current densities; (b)

4 Charge-discharge curves of CPB-based cathode at several current densities; (c) Cycle

5 performances of LiFePO₄ cathodes with PVDF and CPB binders at 0.2C rate between

6 +2.8 to +4.2 V (vs. Li/Li⁺); (d) discharge capacity retention at various discharging

7 current densities of LiFePO₄ electrode with PVDF and CPB at 0.2C charging rate

8 between +2.8 to +4.2 V (vs. Li/Li⁺).

9 EIS was carried out on a cell SS/membrane/SS to determine the ionic conductivity

10 of the CPB and PVDF (saturated with liquid electrolyte). The Nyquist plot of the EIS

11 at 25°C is shown in Fig.5b and Fig.S6. Based on Eq. (1), the obtained ionic

12 conductivities were found to be 3.9 and 0.5×10⁻³ mS cm⁻¹ for the CPB and PVDF,

13 respectively. The ionic conductivity values are consistent with those previously

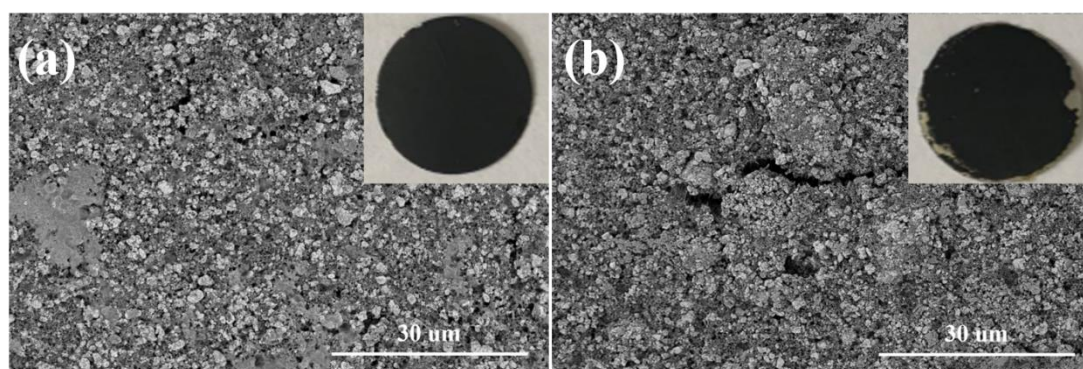
14 obtained in other reports, showing that the PVDF is a non-conductive binder [5, 7-9].

1 The excellent electrochemical performance of the CPB is mainly attributed to the
2 unique structure design of the polymer binder. The anions used as building blocks
3 provide abundant surface-charged $-\text{SO}_3^-$ on the side chains allowing an increase in
4 Li^+ diffusion. This is due to the fact that the single ion conductor characteristics give
5 rise to high mobility of lithium ions in the charge/discharge processes contributing to
6 an improvement of the ionic conductivity [49, 50].

7 *3.2.2 Cell performances*

8 To confirm the improved electrochemical performance of CPB as cathode, the
9 electrodes using different binders were prepared and tested for cell performances,
10 which included charge-discharge profiles, discharge C-rate capability and cyclability,
11 as shown in Fig.6. As expected, the CPB shows higher discharge capacities than the
12 commercial PVDF at various discharge current densities. The initial discharge and
13 charge capacities (at a discharge current density = 0.2 C) of the PVDF and the CPB
14 electrode were observed in the first (1st) cycle at around 140.6mAh/g and 148.5mAh
15 g^{-1} respectively. From Fig.6, it can be observed that the discharge capacity of PVDF
16 electrode dropped rapidly in the 30th cycles and then decreased to below 124.0mAh g^{-1}
17 after the 100th cycle, in contrast to 139.1mAh g^{-1} after 100th cycle for the CPB electrode.
18 This observation may be attributed to the severe exfoliation of the active materials from
19 the current collector caused by the poor adhesion ability of the PVDF binder. Moreover,
20 it was found that the capacity retention of CPB and PVDF after 100 cycles was 94.5%
21 and 87.0% (vs. the initial specific capacity 148.5mAh g^{-1}), respectively (Fig.6c). Fig.6d
22 shows that the CPB exhibits slightly higher discharge capacities than the commercial

1 PVDF binder at different discharge current densities. In this study, it was previously
2 observed that the CPB exhibited a unique 3D hierarchical walnut kernel shape structure,
3 a strong adhesive strength and conducts Li^+ ability inside the cathode, providing higher
4 ionic conductivity, when compared to the commercial PVDF binder. From the
5 electrochemical data, the CPB electrode exhibited better performance than that of the
6 PVDF electrode, indicating that the anion polymer binder can effectively keep the
7 active film adhered to the current collector in a stable manner and accelerate the Li^+
8 diffusion in electrodes, thus improving the electrochemical performance of LiFePO_4
9 cathodes.



10
11 **Fig.7.** Surface morphologies of the cathodes with CPB (a) and PVDF (b) after 100
12 cycle, wherein the inset is a photograph of the LiFePO_4 electrode after 100 cycles.

13 3.2.3 Morphological stability

14 The surface morphology of binder-based cathode was characterized using SEM to
15 study the change in the physical structure before and after cycling. Fig.7 shows the
16 SEM images of the cathodes made of CPB and PVDF after 100 cycles. A uniform
17 particle distribution for CPB (Fig. 7a) was observed whereas small cracks were formed
18 in the PVDF samples (Fig. 7b) after 100 cycles. From these observations, it can be

1 stated that the CPB shows partial healing capabilities. The cracks usually affect the
2 electrode mechanical integrity and the electronic conductivity, yielding a gradual loss
3 of the active LiFePO_4 , and finally a rapid capacity degradation [37]. The inset in Fig.7a
4 and Fig.7b show the photographs of the electrode based on CPB and PVDF after 100
5 cycles. It can be observed that the PVDF-based electrode is detached from the
6 aluminum current collector, while the CPB-based electrode is tightly stuck to it. In this
7 case it may be possible to infer that water-based CPB can help dispersing LiFePO_4 and
8 the conducting material homogeneously during cycling. The homogeneous distribution
9 of active composites could be a reason for good electrical conductivity and stable
10 cycling performance. Moreover, the 3D hierarchical walnut kernel shape structure of
11 the CPB could provide multi-dimensional interactions with active material particle
12 surfaces through the crowded and bulky side groups, enabling the binder to maintain the
13 interactions with LiFePO_4 particles and self-healing property during the charge-
14 discharge cycling process. More importantly, the existence of the $-\text{SO}_3^-$ can deliver
15 the diffusion of the Li^+ out of the cathode, thus improving the electrochemical
16 performance (Fig.S7).

17 **4. Conclusions**

18 A 3D hierarchical walnut kernel shape conductive polymer binder with a $-\text{SO}_3^-$ as
19 an effective aqueous binder via emulsion polymerization was prepared. It was found
20 that the unique 3D hierarchical walnut kernel shape structure of the CPB helped multi-
21 dimensional contacts with the active materials and the conducting agents via non-
22 covalent or covalent interactions. The massive functional nitrile and ether groups of the

1 CPB contributed to improved interactions between the active materials and the
2 conducting agents as well as bonding the active materials on the aluminum current
3 collector. It was also found that the introduced $-\text{SO}_3^-$ played an important role in
4 providing Li^+ pathway and reducing electrical resistance during the charge-discharge
5 cycling process. The 3D hierarchical walnut kernel shape structure, Li^+ conductive
6 channels, along with the superior adhesive strength, contributed to imparting a
7 satisfactory cycling performance and rate capability compared to the cathodes made of
8 PVDF binder. Moreover, the new low cost and eco-friendly water-based binder was
9 easy to prepare. Therefore, it is possible for the CPB material to be recommended as a
10 promising alternative candidate material to a conventional binder for LIBs.

11 **Acknowledgments**

12 This work is supported by National Natural Science Foundation of China (No.
13 51603049, 21766005), Natural Science Foundation of Gui zhou Province (Grant No.
14 [2015] 2059, [2015] 2069).

15 **References**

- 16 [1] P.G. Bruce, S.A. Freunberger, L.J. Hardwick, J.M. Tarascon, Nat. Mater., 11 (2012)
17 19-29.
- 18 [2] H. Xia, Q. Xia, B. Lin, J. Zhu, J.K. Seo, Y.S. Meng, Nano Energy, 22 (2016) 475-
19 482.
- 20 [3] R. Prasanth, V. Aravindan, M. Srinivasan, J. Power Sources, 202 (2012) 299-307.
- 21 [4] I. Kovalenko, B. Zdyrko, A. Magasinski, B. Hertzberg, Z. Milicev, R. Burtovyy, I.

- 1 Luzinov, G. Yushin, *Science*, 334 (2011) 75-79.
- 2 [5] L. Luo, Y. Xu, H. Zhang, X. Han, H. Dong, X. Xu, C. Chen, Y. Zhang, J. Lin, *ACS*
3 *Appl. Mater. Interfaces*, 8 (2016) 8154-8161.
- 4 [6] G. Xu, Q.-b. Yan, A. Kushim, X. Zhang, J. Pana, JuLi, *Nano Energy*, 31 (2017) 568-
5 574.
- 6 [7] G. Xu, B. Ding, J. Pan, P. Nie, L. Shen, X. Zhang, *J. Mater. Chem. A*, 2 (2014)
7 12662-12676.
- 8 [8] J. Wang, Z. Yao, C.W. Monroe, J. Yang, Y. Nuli, *Adv. Funct. Mater.*, 23 (2013) 1194-
9 1201.
- 10 [9] H. Zhong, A. He, J. Lu, M. Sun, J. He, L. Zhang, *J. Power Sources*, 336 (2016) 107-
11 114.
- 12 [10] Pier Paolo Prosini , Maria Carewska , Cinzia Cento, A. Masci, *Electrochim. Acta*,
13 150 (2014) 129-135.
- 14 [11] H.-K. Park, B.-S. Kong, E.-S. Oh, *Electrochem. Commun.*, 13 (2011) 1051-1053.
- 15 [12] U.K. Sen, S. Mitra, *Nano energy*, 5 (2013) 1240-1247.
- 16 [13] D. Shin, HyunjungPark, U. Paik, *Electrochem. Commun.*, 77 (2017) 103-106.
- 17 [14] M. Ling, J. Qiu, S. Li, H. Zhao, G. Liu, S. Zhang, *J. Mater. Chem. A*, 1 (2013)
18 11543.
- 19 [15] M.J. Lacey, F. Jeschull, K. Edstrom, D. Brandell, *Chem. Commun.*, 49 (2013)
20 8531-8533.
- 21 [16] T. Qiu, H. Shao, W. Wang, H. Zhang, A. Wang, Z. Feng, Y. Huang, *RSC Adv.*, 6
22 (2016) 102626-102633.

- 1 [17] Z. Zhang, T. Zeng, Y. Lai, M. Jia, J. Li, *J. Power Sources*, 247 (2014) 1-8.
- 2 [18] B. Koo, H. Kim, Y. Cho, K.T. Lee, N.S. Choi, J. Cho, *Angew. Chem. Int. Ed.*, 51
3 (2012) 8762-8767.
- 4 [19] Y. Bie, J. Yang, Y. Nuli, J. Wang, *J. Mater. Chem. A*, 5 (2017) 1919-1924.
- 5 [20] D. Liu, Y. Zhao, R. Tan, L.-L. Tian, Y. Liu, H. Chen, F. Pan, *Nano Energy*, 36 (2017)
6 206-212.
- 7 [21] G. Liu, S. Xun, N. Vukmirovic, X. Song, P. Olalde-Velasco, H. Zheng, V.S.
8 Battaglia, L. Wang, W. Yang, *Adv Mater*, 23 (2011) 4679-4683.
- 9 [22] H. Zhao, Y. Wei, R. Qiao, C. Zhu, Z. Zheng, M. Ling, Z. Jia, Y. Bai, Y. Fu, J. Lei,
10 X. Song, V.S. Battaglia, W. Yang, P.B. Messersmith, a.G. Liu, *Nano Letter*, 15 (2015)
11 7927-7932.
- 12 [23] S.J. Park, H. Zhao, G. Ai, C. Wang, X. Song, N. Yuca, V.S. Battaglia, W. Yang, G.
13 Liu, *J Am Chem Soc*, 137 (2015) 2565-2571.
- 14 [24] H. Zhao, Z. Wang, P. Lu, M. Jiang, F. Shi, X. Song, Z. Zheng, X. Zhou, Y. Fu, G.
15 Abdelbast, X. Xiao, Z. Liu, V.S. Battaglia, K. Zaghbi, G. Liu, *Nano Lett*, 14 (2014)
16 6704-6710.
- 17 [25] M. Wu, X. Xiao, N. Vukmirovic, S. Xun, P.K. Das, X. Song, P. Olalde-Velasco, D.
18 Wang, A.Z. Weber, L.-W. Wang, V.S. Battaglia, W. Yang, G. Liu, *J. Am. Chem. Soc.*,
19 135 (2013) 12048-12056.
- 20 [26] J. Song, M. Zhou, R. Yi, T. Xu, M.L. Gordin, D. Tang, Z. Yu, M. Regula, D. Wang,
21 *Adv. Funct. Mater.*, 24 (2014) 5904-5910.
- 22 [27] Q. Shi, L. Xue, Z. Wei, F. Liu, X. Du, D.D. DesMarteau, *J. Mater. Chem. A*, 1

- 1 (2013) 15016-15021.
- 2 [28] Z.P. Cai, Y. Liang, W.S. Li, L.D. Xing, Y.H. Liao, *J. Power Sources*, 189 (2009)
- 3 547-551.
- 4 [29] D.-X. Yan, H. Pang, B. Li, R. Vajtai, L. Xu, P.-G. Ren, J.-H. Wang, Z.-M. Li, *Adv.*
- 5 *Funct. Mater.*, 25 (2015) 559-566.
- 6 [30] C. Wu, X. Huang, G. Wang, L. Lv, G. Chen, G. Li, P. Jiang, *Adv. Funct. Mater.*, 23
- 7 (2013) 506-513.
- 8 [31] Y.K. Jeong, T.W. Kwon, I. Lee, T.S. Kim, A. Coskun, J.W. Choi, *Nano Lett*, 14
- 9 (2014) 864-870.
- 10 [32] H. Li, Xuhong Peng, L. Wu, M. Jia, H. Zhu, *J. Phys. Chem. C*, 113 (2009) 4419-
- 11 4425.
- 12 [33] L. Zhang, H. Gao, Y. Liao, *React. Funct. Polym.*, 104 (2016) 53-61.
- 13 [34] T. Chen, Y. Liao, X. Wang, X. Luo, X. Li, W. Li, *Electrochim. Acta*, 191 (2016)
- 14 923-932.
- 15 [35] X. Ma, X. Huang, J. Gao, S. Zhang, Z. Deng, J. Suo, *Electrochim. Acta*, 115 (2014)
- 16 216-222.
- 17 [36] Y. Peng, P. Wu, *Polymer*, 45 (2004) 5295-5299.
- 18 [37] F. Zeng, W. Wang, A. Wang, K. Yuan, Z. Jin, Y.-s. Yang, *ACS Appl. Mater.*
- 19 *Interfaces*, 7 (2015) 26257-26265.
- 20 [38] Naoaki Yabuuchi, Keiji Shimomura, Yukako Shimbe, Tomoaki Ozeki, Jin-Young
- 21 Son, Hiroshi Oji, Yasushi Katayama, Takashi Miura, S. Komaba, *Adv. Energy Mater.*,
- 22 1 (2011) 759-765.

- 1 [39] H. Oh, K. Xu, H.D. Yoo, D.S. Kim, C. Chanthad, G. Yang, J. Jin, I.A. Ayhan, S.M.
2 Oh, Q. Wang, Chem. Mater., 28 (2016) 188-196.
- 3 [40] Z. Zhang, T. Zeng, C. Qu, H. Lu, M. Jia, Y. Lai, J. Li, Electrochim. Acta, 80 (2012)
4 440-444.
- 5 [41] C. Wang, H. Wu, Z. Chen, M.T. McDowell, Y. Cui, Z. Bao, Nat Chem, 5 (2013)
6 1042-1048.
- 7 [42] S. Hu, Y. Li, J. Yin, H. Wang, X. Yuan, Q. Li, Chem. Eng. J., 237 (2014) 497-502.
- 8 [43] L.L.Chai, L.Zhang, Q.T.Qu, H.H.Zheng, Chemistry Bulletin, 76 (2013) 299-306..
9 [44] S.S. Zhang, T.R. Jow, J. Power Sources, 109 (2002) 422-426.
- 10 [45] J. He, J. Wang, H. Zhong, J. Ding, L. Zhang, Electrochim. Acta, 182 (2015) 900-
11 907.
- 12 [46] PhBiensana, BSimonaJ.PPérèsa, Ade Guiberta, MBrousselyb, J.MBodetb,
13 FPertonb, J. Power Sources, (1999) 906-912.
- 14 [47] Z.Zhang, D.Fouchard, J.R.Rea, J. Power Sources, 70 (1998) 16-20.
- 15 [48] Xuning Feng, Minggao Ouyang, Xiang Liu, Languang Lu, Yong Xia, X. He,
16 Energy Storage Materials, 10 (2018) 246-267.
- 17 [49] M. Egashira, H. Todo, N. Yoshimoto, M. Morita, J. Power Sources, 178 (2008)
18 729-735.
- 19 [50] Y. Liu, Y. Zhang, M. Pan, X. Liu, C. Li, Y. Sun, D. Zeng, H. Cheng, J. Membrane
20 Sci., 507 (2016) 99-106.
- 21